Diphenyldihydropentalenediones: Wide Singlet−Triplet Energy Gap Compounds Possessing the Planarly Fixed Diene Subunit

Tomoki Nagaoka, Yasunori Matsui,* Masaaki Fuki, Takuya Ogaki, Eisuke Ohta, Yasuhiro Kobori, and Hiroshi Ikeda*

ACCESS | 📊 Metrics & More | 📖 Article Recommendations | 🅂🄸 Supporting Information

ABSTRACT: 2,2,5,5-Tetramethyl-3,6-diphenyl-2,5-dihydropentalene-1,4-dione (PD-H) and its dimethoxy (PD-OCH$_3$) and bis-(trifluoromethyl) derivatives (PD-CF$_3$) were developed as a new class of compounds possessing a wide excited singlet−triplet energy gap. The PD derivatives would also have a high energy level of the triplet-excited state (E_T) due to the planarity of the fused-diene subunit. The results of photophysical studies revealed that the energy level of the singlet-excited state (E_S) and E_T of PD-H are 2.88 and 1.43 eV, respectively. These values indicate that PD-H has the energy relationship, $E_S > 2E_T$, required for it to be a singlet fission (SF) material. Moreover, the introduction of electron-donating or -withdrawing groups on the benzene rings in PD-H enables fine-tuning of E_S and E_T. The results of transient absorption spectroscopic studies show that PD-H, PD-OCH$_3$, and PD-CF$_3$ in CH$_2$Cl$_2$ have respective T$_1$ lifetimes of 71, 118, and 107 μs, which are long enough to utilize its triplet exciton in other optoelectronic systems. These findings suggest that the PDs are potential candidates for SF materials with high E_T levels.
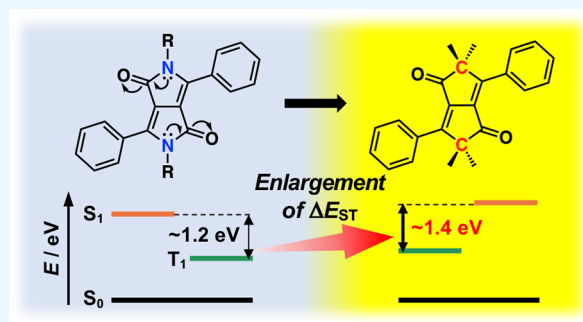
INTRODUCTION

In the optoelectronic material development, the design and control of singlet- (S$_1$) and triplet-excited state (T$_1$) energy levels (E_S and E_T, respectively, Figure 1) are the fundamentals.
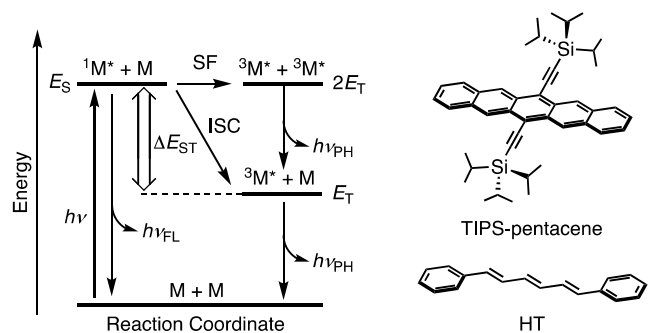

Figure 1. (left) Jablonski diagram showing the generation of two ^{3}M* by SF and the importance of ΔE_{ST}. (right) Chemical structures of TIPS-pentacene and HT.

Especially, the gap between E_S and E_T (=ΔE_{ST}) is an important factor in the molecular design for thermally activated delayed fluorescence (FL),[1,2] photon upconversion,[3−6] and singlet fission (SF).[7,8] SF is a photophysical process in which an intermolecular interaction between S$_1$ and ground-state (S$_0$) molecules (^{1}M* and M, respectively) generates two T$_1$ species (^{3}M*). The process, which proceeds via a correlated triplet

pair [TT],[9−11] is depicted in terms of multiplicity changes in eq 1.

$$S_1 + S_0 \rightarrow [TT] \rightarrow T_1 + T_1 \tag{1}$$

Importantly, because SF increases the quantum yield of ^{3}M* formation up to a maximum of 200%, it is a promising method to improve the efficiencies of photovoltaic devices.[12,13] Consequently, over the past several years, many experimental and theoretical investigations have been conducted to uncover new SF materials.[14−27]

To achieve the proper exergonicity for efficient SF, E_S of a substance must be higher than twice E_T (i.e., $E_S > 2E_T$). By considering ΔE_{ST}, the relationship can be converted into eq 2

$$E_S - E_T = \Delta E_{ST} > E_T \tag{2}$$

which indicates that a large ΔE_{ST} is also required for exergonic SF. From the viewpoint of solar cell applications, desirable SF materials with high E_T can be used in combination with semiconductors such as Si[28,29] and Pb perovskite[30,31] that have

high power conversion efficiencies. Quantitatively, ΔE_{ST} can be expressed by eq 3[32]

$$\Delta E_{ST} \approx 2 \iint \varphi_H(\boldsymbol{r}_1)\varphi_L(\boldsymbol{r}_2)\frac{e^2}{|\boldsymbol{r}_2 - \boldsymbol{r}_1|}\varphi_H(\boldsymbol{r}_2)\varphi_L(\boldsymbol{r}_1)\mathrm{d}\boldsymbol{r}_1\mathrm{d}\boldsymbol{r}_2$$

(3)

where φ_H and φ_L are wavefunctions of the respective highest occupied molecular orbital (HOMO) and lowest unoccupied molecular orbital (LUMO) of a substance, and $\boldsymbol{r}_1$ and $\boldsymbol{r}_2$ are spatial coordinates. This relationship shows that enhancement of ΔE_{ST} can be effectively achieved by increasing the overlap between the HOMO and LUMO. The well-known SF material, 6,13-bis(triisopropylsilylethynyl)pentacence[33,34] (TIPS-pentacene, Figure 1) has a relatively large ΔE_{ST} of *ca.* 1.1 eV[35] owing to the existence of significant spatial HOMO−LUMO overlap.

One strategy used to increase ΔE_{ST} (and E_T) involves incorporation of a linearly conjugated polyene system, similar to those present in conventional SF materials including carotenes[36−38] and arylated polyenes such as *trans,trans,trans*-1,6-diphenylhexatriene (HT, Figure 1).[39−41] However, polyenes of this type undergo facile $E-Z$ photoisomerization[42] and [2+2] photocyclodimerization[43] reactions. Thus, these excited state decay pathways need to be blocked by using ring constraints and/or bulky substituents. Examples of a ring-fused polyene containing SF material of this type is 2,5-dihydropyrrolo[3,4-*c*]pyrrole-1,4-dione (PP) derivatives, such as the 3,6-dithienyl derivative (PP-Th, Figure 2) and the 3,6-
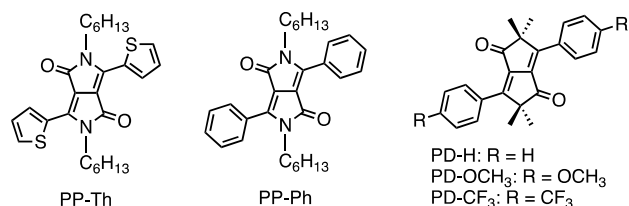

Figure 2. Chemical structures of PP-Th, PP-Ph, and the PDs (PD-H, PD-OCH₃, and PD-CF₃).

diphenyl derivative (PP-Ph, Figure 2).[44] However, the PPs possess the disadvantageous feature of having relatively small ΔE_{ST}[45] and E_T values, which are probably a consequence of the contribution of a zwitterionic resonance structure in the two amide moieties.

These observations led us to reason that 2,2,5,5-tetramethyl-3,6-diphenyl-2,5-dihydropentalene-1,4-dione (PD-H, Figure 2), a carbon analogue of PP-Ph, and its dimethoxy (PD-OCH₃) and bis(trifluoromethyl) (PD-CF₃) derivatives have the potential of being new types of wide ΔE_{ST} substances. The dihydropentalenedione core in this PD family (PDs) contains a diene moiety that should enhance ΔE_{ST} and a ring fusion constraint that should make it more photochemically stable than a naked diene. In addition, PD-H and its derivatives should have high E_T values owing to the absence of amide groups and zwitterionic resonance structures. Moreover, we anticipated that an introduction of electron-donating methoxy and electron-withdrawing trifluoromethyl groups on the benzene rings of PD-H would enable fine-tuning of E_S, E_T, and ΔE_{ST}. In the study described below, we prepared PD-H, PD-OCH₃, and PD-CF₃ and examined their photophysical properties using time-resolved spectroscopy. The results demonstrated that the diphenyldihydropentalenedione frame-

work exhibits a wide ΔE_{ST} and is a potential candidate for new SF materials with high E_T values.

■ EXPERIMENTAL SECTION

General. Melting points (mp) were obtained with a Yanaco MP-500 apparatus and are all uncorrected. Preparative gel permeation chromatography was conducted on Japan Analytical Industry LC-918 with JAIGEL-1H styrene-based polymers. ¹H, ¹³C, and ¹⁹F NMR spectra were recorded at 400, 100, and 376 MHz, respectively, on a Bruker AVANCE NEO 400 spectrometer. Chemical shifts (δ) are reported in ppm using the signals of $(CH_3)_4Si$ (0 ppm), $CDCl_3$ (77.0 ppm), and C_6F_6 (−163.0 ppm) as respective internal standards for ¹H, ¹³C, and ¹⁹F NMR. IR spectra were recorded on a JASCO FT/IR 8300 spectrometer using the liquid film method with NaCl plates and the attenuated total reflection (ATR) method. Low-resolution atmospheric solid analysis probe mass measurements were carried out with a Shimadzu LCMS-2020 mass spectrometer and LabSolutions LCMS software. High-resolution (HR) electrospray ionization mass measurements were carried out with a Bruker micrOTOF system after calibration using an HCO₂Na solution. Elemental analyses were carried out at the Analytical Center, Graduate School of Science, Osaka Metropolitan University. UV−vis absorption spectra of solutions were recorded using a JASCO V-570 spectrometer, and those of crystals were recorded using the waveguide technique on a System Instruments SIS-5000 waveguide spectrometer. Photoluminescence spectra were recorded on a JASCO FP-8500 spectrometer. Absolute FL quantum yields (Φ_{FL}) were determined using the integrating sphere method along with a Hamamatsu Photonics C9920-02 absolute photoluminescence quantum yield measurement system. FL decay profiles were measured by using a HORIBA Jobin Yvon FluoroCube lifetime spectrofluorometer equipped with HORIBA NanoLED-370 and analyzed using DAS6 FL decay analysis software.

Preparation of Substances. The PDs (PD-H, PD-OCH₃, and PD-CF₃) were synthesized using the sequences shown in Scheme 1. Details for the preparation of intermediates **2**, **3**, **4**, and **5** are given in the Supporting Information.

Scheme 1. Sequences for the Synthesis of the PDs
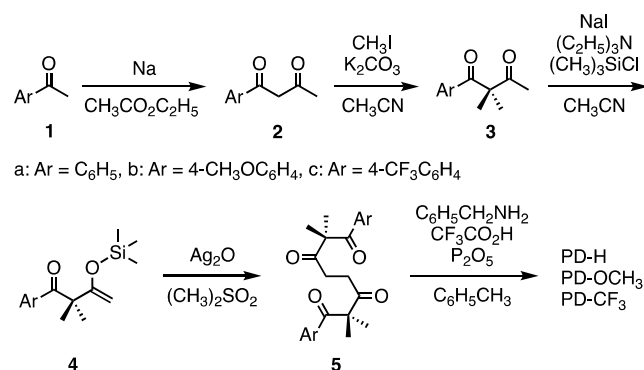
2,2,5,5-Tetramethyl-3,6-diphenyl-2,5-dihydropentalene-1,4-dione (PD-H). To a 100 mL round-bottom flask were added **5a** (0.90 g, 2.4 mmol), C₆H₅CH₂NH₂ (0.26 g, 2.4 mmol), P₂O₅ (3.6 g, 2.9 mmol), and toluene (C₆H₅CH₃, 31 mL). CF₃CO₂H (0.32 g, 2.9 mmol) was then added at 0, 7, 21, 31, 45, 55, and 69 h after initiation of the reaction. Following

stirring at reflux for 76 h, the mixture was diluted with 25 mL of $C_6H_5CH_3$ and filtered. The filtrate was washed with saturated aqueous Na_2CO_3 (25 mL) followed by water (13 mL). Also, the gel containing P_2O_5 was carefully washed with $C_6H_5CH_3$ (20 mL) and water (50 mL). The combined organic layers were dried over anhydrous Na_2SO_4 and concentrated under reduced pressure. The residue was subjected to silica-gel column chromatography (ϕ 4.0 cm, h 20 cm, eluent n-hexane/ $CHCl_3$ = 1/1) and the resulting solid was recrystallized from C_2H_5OH to give pure PD-H (0.39 g, 1.1 mmol) as pale yellow needles in 48% yield. mp 220−220.5 °C; ^1H NMR (400 MHz, $CDCl_3$): δ_{ppm} 1.52 (s, 12H), 7.40−7.48 (m, 6H), 7.95 (AA′BB′C, J = 8.0, 2.0 Hz, 4H); ^{13}C NMR (100 MHz, $CDCl_3$): δ_{ppm} 24.2 (4C), 60.9 (2C), 128.4 (2C), 129.2 (4C), 130.1 (4C), 132.8 (2C), 138.7 (2C), 151.6 (2C), 203.6 (2C); IR (ATR, neat) ν/cm^{-1}: 2975, 2935, 2873, 1712 (C=O), 1054, 752, 686; HRMS (ESI) m/z: [M + Na]$^+$ calcd for $C_{24}H_{22}O_2Na$, 365.1512; found, 365.1512; Anal. Calcd for $C_{24}H_{22}O_2$: C, 84.18; H, 6.48. Found: C, 84.12; H, 6.56.

2,2,5,5-Tetramethyl-3,6-bis(4-methoxyphenyl)-2,5-dihy-dropentalene-1,4-dione (PD-OCH₃). PD-OCH$_3$ was synthesized in 43% yield from **5b** using a similar procedure. Yellow blocks, mp 235−235.5 °C (C_2H_5OH); ^1H NMR (400 MHz, $CDCl_3$): δ_{ppm} 1.54 (s, 12H), 3.87 (s, 6H), 6.97 (AA′XX′, J = 9.0, 2.6 Hz, 4H), 8.08 (AA′XX′, J = 9.0, 2.6 Hz, 4H); ^{13}C NMR (100 MHz, $CDCl_3$): δ_{ppm} 24.4 (4C), 55.4 (2C), 60.7 (2C), 113.8 (4C), 125.7 (2C), 131.2 (4C), 137.1 (2C), 150.5 (2C), 161.0 (2C), 204.1 (2C); IR (ATR, neat) ν/cm^{-1}: 2974, 2936, 1699 (C=O), 1600, 1508, 1260, 1252, 1177, 1056, 831; HRMS (ESI) m/z: [M + Na]$^+$ calcd for $C_{26}H_{26}O_4Na$, 425.1723; found, 425.1723; Anal. Calcd for $C_{26}H_{26}O_4$: C, 77.59; H, 6.51. Found: C, 77.60; H, 6.58.

2,2,5,5-Tetramethyl-3,6-bis[4-(trifluoromethyl)phenyl]-2,5-dihydropentalene-1,4-dione (PD-CF₃). PD-CF$_3$ was synthesized in 5% yield from **5c** using a similar procedure. Pale yellow prisms, mp 295−296 °C (C_2H_5OH); ^1H NMR (400 MHz, $CDCl_3$): δ_{ppm} 1.53 (s, 12H), 7.71 (AA′XX′, J = 8.4 Hz, 4H), 8.03 (AA′XX′, J = 8.4 Hz, 4H); ^{13}C NMR (100 MHz, $CDCl_3$): δ_{ppm} 24.0 (4C), 61.0 (2C), 123.8 (q, J_{CF} = 270.5 Hz, 2C), 125.4 (q, J_{CF} = 3.7 Hz, 4C), 129.4 (4C), 131.7 (q, J_{CF} = 21.7 Hz, 2C), 135.8 (2C), 139.9 (2C), 150.7 (2C), 202.7 (2C); ^{19}F NMR (376 MHz, $CDCl_3$): δ_{ppm} −64.29 (s, 6F); IR (ATR, neat) ν/cm^{-1}: 2967, 2932, 2872, 1719 (C=O), 1323, 1113; HRMS (ESI) m/z: [M + Na]$^+$ calcd for $C_{26}H_{20}F_6O_2Na$, 501.1260; found, 501.1262; Anal. Calcd for $C_{26}H_{20}F_6O_2$: C, 65.27; H, 4.21. Found: C, 65.27; H, 4.30. Together with **5c**, the product of Paal−Knorr reaction, 2,5-bis[2-methyl-1-(4-trifluoromethylphenyl)propan-1-one-2-yl]furan, was also formed in 59% yield. Colorless powder. mp 59.5−61 °C (C_2H_5OH); ^1H NMR (400 MHz, $CDCl_3$): δ_{ppm} 1.48 (s, 12H), 6.25 (s, 2H), 7.46 (AA′BB′, J = 8.6 Hz, 4H), 7.52 (AA′BB′, J = 8.6 Hz, 4H); ^{13}C NMR (100 MHz, $CDCl_3$): δ_{ppm} 25.2 (4C), 48.2 (2C), 106.5 (2C), 123.4 (q, J_{CF} = 270.9 Hz, 2C), 125.0 (q, J_{CF} = 3.6 Hz, 4C), 128.6 (4C), 133.0 (q, J_{CF} = 32.6 Hz, 2C), 139.9 (2C), 157.4 (2C), 200.8 (2C); ^{19}F NMR (376 MHz, $CDCl_3$): δ_{ppm} −64.56 (s, 6F); IR (ATR, neat) ν/cm^{-1}: 1682 (C=O), 1647, 1326, 1124, 1066; HRMS (ESI) m/z: [M + Na]$^+$ calcd for $C_{26}H_{22}F_6O_3Na$, 519.1365; found, 519.1370.

Theoretical Calculations. Density functional theory (DFT) calculations were carried out using a Gaussian 09W[46] program with a (U)B3LYP functional and 6-31+G** basis set. All the geometries were successfully optimized to afford no imaginary frequencies.

X-ray Crystallographic Analysis. Single-crystal X-ray crystallographic analysis was performed using a Rigaku R-AXIS RAPID diffractometer. The initial structural model was resolved by the intrinsic phasing method (SHELXT)[47] and was refined by using the least-square method of the squared amplitudes of the structure factor (SHELXL).[48] Non-hydrogen atoms were refined using an anisotropic temperature factor, and the hydrogen atoms are fixed to the positions calculated by the riding model. Olex2 Version 1.3.0 program[49] was used for all analysis.

Absorption and FL Measurements. UV−vis absorption and FL spectra of degassed CH_2Cl_2 solutions (2×10^{-5} M) were obtained by using a 10 mm pathlength quartz cuvette at room temperature. Absorption spectra of crystals were recorded on a quartz surface under air by using slab optical waveguide spectroscopy. A 150 W Xe arc lamp was used as the probe light source. Photoluminescence spectra of crystals were recorded under degassed conditions at room temperature. The crystals were excited at their absorption maxima. Absolute Φ_{FL} were determined under argon at room temperature by using the integrating sphere method. Samples were excited at their absorption maxima.

S₀−T₁ Absorption Measurements. Following the method described in the literature,[50] S_0−T_1 absorption spectra were recorded using solutions in the heavy atom containing solvent C_2H_5I (aerated) containing highly concentrated samples (*ca.* 0.1 M) and a 20 mm pathlength quartz cuvette at room temperature using a UV−vis−NIR spectrophotometer equipped with photomultiplier and PbS detectors.

FL Lifetime Measurements. FL lifetime (τ_{FL}) measurements were carried out on degassed CH_2Cl_2 solutions (2×10^{-5} M) in a 10 mm pathlength quartz cuvette or for crystals on a quartz Petri dish at room temperature. The samples were excited at 371 nm with a 1 MHz repetition frequency. The values of τ_{FL} were obtained by using the time-correlated single-photon counting technique.

Nanosecond Absorption Spectroscopy. Nanosecond absorption spectroscopy was carried out using a UNISOKU USP-T1000 system. An Nd/YAG pulsed laser (Continuum, Surelite-3) equipped with an optical parametric amplifier (410−700 nm) and a 150 W Xe arc lamp were used as the respective excitation and monitoring light sources. The degassed CH_2Cl_2 solutions (2×10^{-5} M) were studied using laser flash photolysis (LFP) with a 10 mm pathlength quartz cuvette at room temperature. Solutions were excited at wavelengths at which samples have absorbances of 0.3−0.6.

RESULTS AND DISCUSSION

Synthesis. 2,5-Dihydropentalene-1,4-dione was first synthesized in 2018[51] by using an intramolecular double cyclization−dehydration reaction of the corresponding tetraone. Using a modification of this approach, we prepared the PDs through five-step sequences starting with the corresponding commercially available acetophenone derivatives (**1**, Scheme 1) or 1-phenylbutane-1,3-dione (**2a**). Specifically, Claisen condensations of the acetophenones **1** with $CH_3CO_2C_2H_5$ generated the respective 1,3-diones **2**,[52−54] which were dimethylated using CH_3I and K_2CO_3 to provide **3**.[54−56] The silyl enol ethers **4**,[57] generated by the treatment of **3** with $(CH_3)_3SiCl$ and $(C_2H_5)_3N$ in the presence of NaI, were oxidatively dimerized using Ag_2O to form tetraones **5**.[57] Finally, intramolecular double cyclization−dehydration reactions of refluxing $C_6H_5CH_3$ solutions of **5** containing

CF$_3$CO$_2$H, C$_6$H$_5$CH$_2$NH$_2$, and P$_2$O$_5$ (drying agent) produced PD-H, PD-OCH$_3$, and PD-CF$_3$ in 48, 43, and 5% respective yields. The low yield of PD-CF$_3$ in this process is associated with the competitive formation of the furan derivative.[58] The structures of the PDs were confirmed by using ^{1}H NMR, ^{13}C NMR, and IR spectroscopy, MS spectrometry, and X-ray crystallographic analysis.

Theoretical Study. The electronic structures of the PDs were assessed using DFT calculations. The results indicate that the optimized geometry of the dihydropentalenedione core and two phenyl groups in PD-H and its derivatives is basically planar. Moreover, the HOMO and LUMO distributions in the PDs greatly overlap (Figure 3). Time-dependent DFT
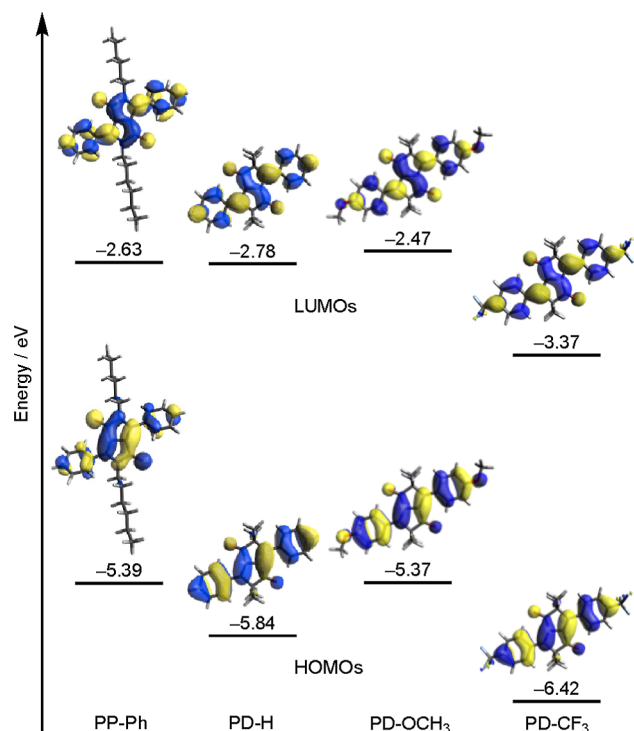

Figure 3. HOMOs and LUMOs of PP-Ph and the PDs calculated by using the B3LYP/6-31+G** level of theory.

calculations with PD-H gave E_S = 2.71 eV and E_T = 1.35 eV (Table 1). The calculated ΔE_{ST} of PD-H is +1.36 eV, which is relatively larger than that of PP-Ph (ΔE_{ST} = +1.27 eV). Also, note that E_S (2.42 eV) and E_T (1.15 eV) of PP-Ph are smaller than those of PD-H, probably associated with zwitterionic resonance structures in the former. DFT calculations showed that, similar to PD-H, PD-OCH$_3$ and PD-CF$_3$ have relatively large E_S, E_T, and ΔE_{ST} values. These results suggest that the presence of a fused-diene subunit and the absence of zwitterionic resonance structures lead to the enlargement of E_T, and the presence of a large spatial overlap of the HOMO and LUMO contributes to enhancing ΔE_{ST} (eq 3).

X-ray Crystallographic Analysis. Because SF is a phenomenon that requires close intermolecular interactions, it ideally takes place in condensed media such as the crystalline state. Therefore, crystal packing information is important in assessing the viability of potential SF materials.[60−64] To gain insights into their molecular and crystal structures, X-ray crystallographic analysis was carried out on the PDs. Suitably high-quality single crystals of PD-H, PD-OCH$_3$, and PD-CF$_3$

Table 1. E_S, E_T, and ΔE_{ST} Values of the PDs and Related Substances

substances	E_S/eV	E_T/eV	ΔE_{ST}/eV
HT	2.96[a]	1.31[a]	+1.65
	3.19[b]	1.49[c]	+1.70
PD-H	2.71[a]	1.35[a]	+1.36
	2.88[d]	1.43[e]	+1.45
PD-OCH$_3$	2.62[a]	1.34[a]	+1.28
	2.70[d]		
PD-CF$_3$	2.67[a]	1.33[a]	+1.34
	2.92[d]		
PP-Ph	2.42[a]	1.15[a]	+1.27
	2.50[f]		
PP-Th	2.25[a]	0.96[a]	+1.29
	2.24[f]	1.1[g]	+1.14
TIPS-pentacene	1.75[h]	0.86[h]	+1.09

[a]By using the B3LYP/6-31+G** level. [b]In a supersonic He jet.[41] [c]In crystals.[41] [d]In degassed CH$_2$Cl$_2$. [e]In C$_2$H$_5$I. [f]In CH$_2$Cl$_2$.[44] [g]In C$_6$H$_5$CH$_3$.[59] [h]In crystals.[35]

were obtained by recrystallization from C$_2$H$_5$OH, CHCl$_3$−CH$_3$OH, and CHCl$_3$−C$_2$H$_5$OH, respectively. Unlike to the DFT calculations, analysis of the crystallographic data (Figure 4) showed that the two benzene rings in these substances are twisted relative to the dihydropentalenedione core, imposed by crystal packing. The dihedral angles between the benzene rings and the dihydropentalenedione core for PD-H, PD-OCH$_3$, and
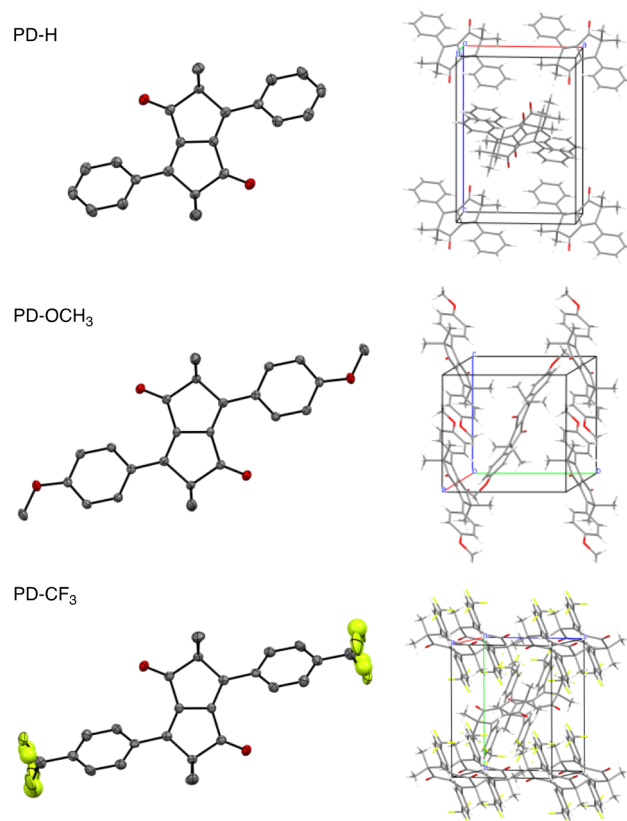

Figure 4. (left) Molecular and (right) crystal structures obtained by X-ray crystallographic analysis of PD-H (CCDC-2164027), PD-OCH$_3$ (-2164028), and PD-CF$_3$ (-2164029) (thermal ellipsoids: 50% probability). Hydrogen atoms in the left graphics are omitted for clarity.

PD-CF$_3$ are 35.4, 25.6, and 44.0°, respectively. In the crystalline state, molecules of PD-H form a herringbone structure (Figure S1a), with intermolecular distances between the benzene ring and the dihydropentalenedione core of an adjacent molecule of *ca.* 4.3 Å. In contrast, crystals of PD-OCH$_3$ do not have this type of stacking pattern (Figure S1c), and PD-CF$_3$ crystals have a slipped stacking structure (Figure S1e), which is likely a result of the dominance of the interaction between an F atom and the fused-diene subunit. These findings indicate that no remarkable $\pi-\pi$ interactions exist in crystals of the PDs. Furthermore, the short intermolecular distances of *ca.* 2.5 Å between the benzene ring hydrogen atoms and the carbonyl oxygen atoms of adjacent molecules suggest that intermolecular CH···O interactions occur in the crystals (Figure S1).

Photophysical Properties. UV–vis absorption spectra of PD-H and PD-CF$_3$ in CH$_2$Cl$_2$ contain bands at 359 nm associated with allowed $\pi-\pi^*$ transitions (Figure 5a and Table
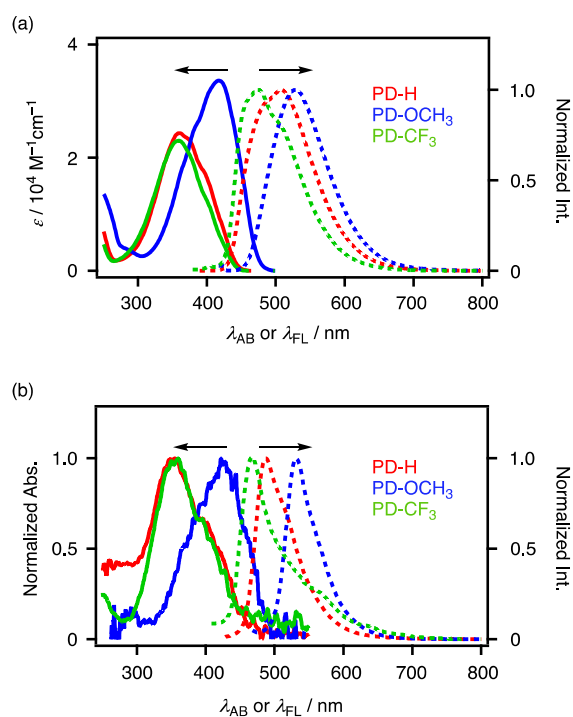

Figure 5. (a) UV–vis absorption (solid line) and FL (dotted line) spectra of the PDs in CH$_2$Cl$_2$ (2×10^{-5} M) (λ_{EX} = 359, 417, and 359 nm for PD-H, PD-OCH$_3$, and PD-CF$_3$, respectively). (b) Waveguide-based absorption and FL spectra of crystals of the PDs (λ_{EX} = 352, 422, and 355 nm for PD-H, PD-OCH$_3$, and PD-CF$_3$, respectively).

2). In contrast, the spectrum of the methoxy derivative PD-OCH$_3$ contains an absorption band at the longer wavelength of

417 nm, which corresponds to its small HOMO–LUMO energy gap (Figure 3).

The FL spectra of CH$_2$Cl$_2$ solutions of PD-H, PD-OCH$_3$, and PD-CF$_3$ contain maxima at 507, 528, and 474 nm, respectively. FL spectra of PD-H and PD-CF$_3$ contain slight vibronic structures corresponding to the carbonyl stretching. On the other hand, emission of PD-OCH$_3$ is structureless, probably because of zwitterionic resonance structures associated with the methoxyphenyl groups and the dihydro-pentalenedione core. Deconvolutions of the UV–vis absorption and FL spectra (Figure S2) using Gaussian functions provided E_S values of 2.88, 2.70, and 2.92 eV for PD-H, PD-OCH$_3$, and PD-CF$_3$, respectively. The observations that PD-CF$_3$ has the highest E_S are likely due to the lack of zwitterionic resonance structures associated with the trifluoromethyl-substituted phenyl groups and the dihydropentalenedione core. The Φ_{FL} values of the PDs in CH$_2$Cl$_2$ solutions are all <0.05. The very short τ_{FL} (<0.5 ns, Figure 7) of these substances indicate the occurrence of a rapid intramolecular quenching process.

The E_T values could not be determined for the PDs in the conventional manner because methylcyclohexane matrices of these substances at 77 K do not phosphoresce. Thus, we employed a spin-forbidden S$_0$–T$_1$ absorption measurement method to obtain the E_T value using a 20 mm quartz cuvette and C$_2$H$_5$I.[50] The principle of S$_0$–T$_1$ absorption measurements is based on the interaction between the magnetic moment of spin and the magnetic field due to the orbital motion of electrons, enhanced by the external heavy atom effect. Because a molar extinction coefficient ε of S$_0$–T$_1$ absorption is quite low (*ca.* 1 M^{-1} cm^{-1}), the resulting optical density (OD) is small. However, it is known that this method is an alternative tool to determine the E_T value of compounds whose triplet state phosphoresces inefficiently or is generated inefficiently by intersystem crossing (ISC). Our measurement of S$_0$–T$_1$ absorption of anthracene (λ_{AB} = 677 nm, 1.83 eV, Figure S5) successfully reproduced E_T reported in the literature (1.85 eV).[65] Although PD-H did not exhibit clear absorption peaks, the S$_0$–T$_1$ absorption spectrum of PD-H contains a weak absorption edge at 865 nm (Figure 6). This value corresponds to E_T = 1.43 eV, which is close to the calculated value (1.35 eV) within the range of possible statistical errors. Notably, the experimental E_T values satisfy the $E_S > 2E_T$ relationship required for exergonic SF. Preliminary quenching experiments of triplet-excited octaethylporphyrin (E_T = 1.61 eV) with PD-H revealed that the energy transfer has efficiently occurred at a rate constant of $k_{ET} = 2.6 \times 10^8$ M^{-1} s^{-1}. This experiment supports that E_T of PD-H is lower than 1.61 eV, indicating that S$_0$–T$_1$ absorption should be observed at >775 nm region (Figure S6).

The photophysical properties of crystals of the PDs were also determined. The absorption spectra of PD-H, PD-OCH$_3$, and PD-CF$_3$ crystals, obtained using a waveguide techni-

Table 2. Photophysical Properties of the PDs

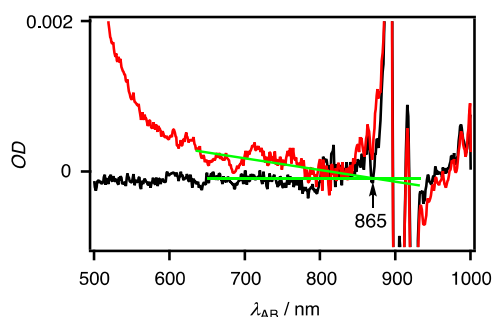|	CH$_2$Cl$_2$ solution[a]					crystals		
PDs	λ_{AB}/nm	ε/10^4 M^{-1} cm^{-1}	λ_{FL}/nm	Φ_{FL}	τ_{FL}/ns	λ_{AB}/nm	λ_{FL}/nm	Φ_{FL}
PD-H	359	2.4	507	0.026	0.4 (58%), <0.1 (42%)	352	487	<0.02
PD-OCH$_3$	417	3.4	528	0.045	0.5 (59%) <0.1 (41%)	422	531	0.282
PD-CF$_3$	359	2.3	474	<0.02	<0.1 (100%)	355	467	<0.02

[a]2×10^{-5} M under argon.

Figure 6. UV−vis absorption spectra of PD-H (*ca.* 0.1 M, red line) and blank (black line) in aerated C_2H_5I. Some spikes at the 900 nm region are associated with harmonics C−H stretching vibration.

que,[66−68] contain maxima at 352, 422, and 355 nm, respectively, that are similar to those of corresponding CH_2Cl_2 solutions (Figure 5b). The FL spectra of PD-H, PD-OCH_3, and PD-CF_3 crystals contain maximum at 487, 531, and 467 nm, respectively, which are also close to those of CH_2Cl_2 solutions. These observations are consistent with the conclusion (see above) that weak intermolecular interactions occur in the crystalline states of the PDs.

The Φ_{FL} values of the PD-H and PD-CF_3 crystals are <0.02, which are similar to those of CH_2Cl_2 solutions. However, PD-OCH_3 in the crystalline state has a relatively large Φ_{FL} of 0.28, which is associated with intense green FL. This behavior clearly shows that suppression of geometrical changes by the crystal lattice decreases the thermal deactivation of S_1 of PD-OCH_3. In this regard, PD-OCH_3 in a tetrahydrofuran/water mixture displays typical aggregation-induced emission (AIE,[69,70] Figure S7). Notably, similar suppression of geometry changes must occur in PD-H and PD-CF_3 crystals, but they do not lead to large Φ_{FL} values and AIE.

To omit the effects of thermal deactivation, FL decay profiles of the PDs was also measured at 77 K. The 2-methyltetrahydrofuran (MTHF) matrices of PD-H and PD-OCH_3 exhibited that ^{1}PD* decays in a single exponential manner (Figure 7d,e) owing to an unimolecular deactivation of ^{1}PD*. In contrast, the PD-CF_3 in the MTHF matrix exhibited a complicated decay profile (Figure 7f). On the other hand, the PD-OCH_3 in crystal, which does not satisfy the $E_S > 2E_T$ requirement, shows a decay profile (τ_{FL} = 2.3 ns) similar to that in the MTHF matrix (Figure 7e). Interestingly, PD-H and PD-CF_3 that satisfy the requirement exhibited more rapid (τ_{FL} = 0.4 ns for PD-H and τ_{FL} < 0.1 ns for PD-CF_3) and slow (τ_{FL} = 5.7 ns for PD-H and τ_{FL} = 4.1 ns for PD-CF_3) decay profiles, respectively (Figure 7d,f). The former will be associated with deactivation such as SF and/or internal conversion, specifically for S_1 of PD-H and PD-CF_3[71,72] and the latter will involve delayed FL.

Nanosecond Absorption Spectroscopy. Nanosecond absorption spectroscopy using LFP was employed to investigate the photophysical properties of the PDs (Figure 8). Photoexcitation of PD-H in degassed CH_2Cl_2 using a 420 nm laser led to the generation of transient absorption bands at 600 and 403 nm, along with the disappearance of the absorption band at 341 nm associated with ground-state PD-H (Figure 8a). The band at 403 nm has a lifetime (τ_T) of 71 μs and decayed following a single exponential function (Figure S8a). Because this long-lived excited species is quenched by using an O_2 atmosphere, it was assigned to the triplet-excited state ^{3}PD-H*. Support for this assignment comes from DFT
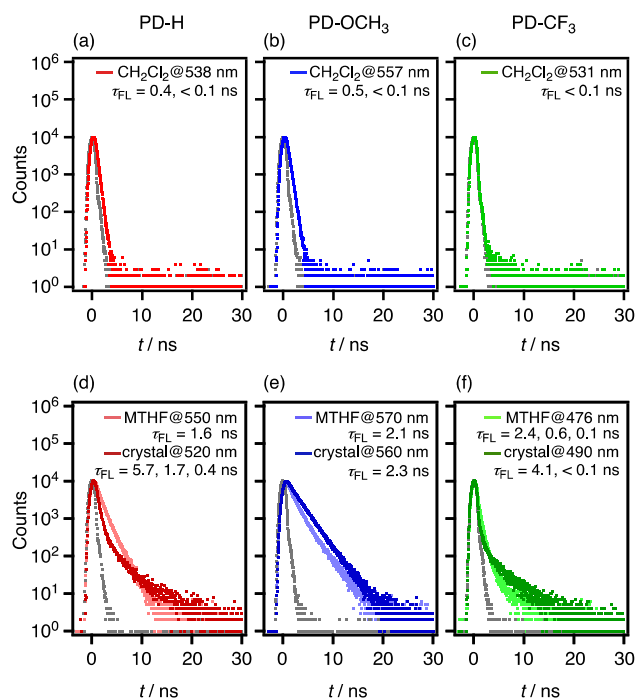

Figure 7. (a−c) FL decay profiles of the PDs (2×10^{-5} M, λ_{EX} = 371 nm) in degassed CH_2Cl_2 at room temperature. (d−f) FL decay profiles of MTHF matrices (2×10^{-5} M) and crystals of the PDs at 77 K. Gray dots are drawn based on the instrumental response functions.
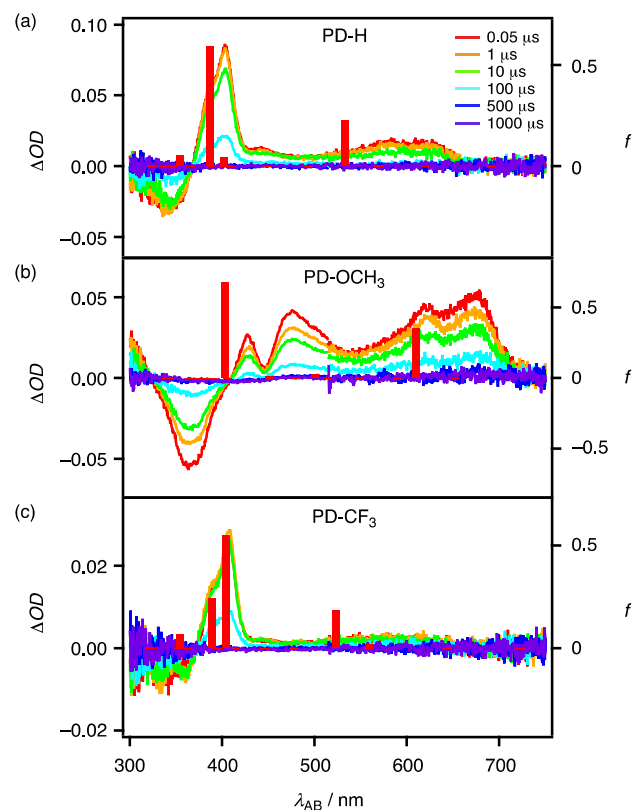

Figure 8. Transient absorption spectra of (a) PD-H, (b) PD-OCH_3, and (c) PD-CF_3 (2×10^{-5} M) in degassed CH_2Cl_2 at room temperature along with calculated electronic transitions (bold red bars, UB3LYP/6-31+G**) for the corresponding ^{3}PDs* (λ_{EX} = 420, 450, and 420 nm for PD-H, PD-OCH_3, and PD-CF_3, respectively).

calculations described above, which indicate that ^{3}PD-H* has electronic transitions at 532 ($f = 0.227$) and 386 nm ($f = 0.592$). Similarly, LFP of PD-OCH$_3$ and PD-CF$_3$ in degassed CH$_2$Cl$_2$ results in the production of transient spectra assignable to ^{3}PD-OCH$_3$* (Figures 8b and S8b, $\tau_T = 118$ μs) and ^{3}PD-CF$_3$* (Figures 8c and S8c, $\tau_T = 107$ μs), respectively. These τ_T values are long enough to utilize their triplet energy as an excitation energy for other optoelectronic systems. A relatively large ΔOD value of PD-OCH$_3$ (Figure 8b) in the longer wavelength region (450−700 nm) compared with PD-H and PD-CF$_3$ is probably due to the zwitterionic resonance structures associated with the methoxyphenyl groups and the dihydropentalenedione core. Because SF does not take place in the dilute solution phase, the process responsible for decay of ^{1}PDs* is most likely ISC. Taking account of the fact that they have large ΔE_{ST} values, the pathway for formation of ^{3}PDs* probably involves the conversion of S$_1$ into a higher triplet-excited state (T$_{n \geq 2}$), followed by internal conversion. Moreover, the preliminary results of a time-resolved electron paramagnetic resonance (EPR) study of PD-H crystals supported the formation of ^{3}PD-H* (Figures 9 and S9). The zero-field splitting parameters $D =$
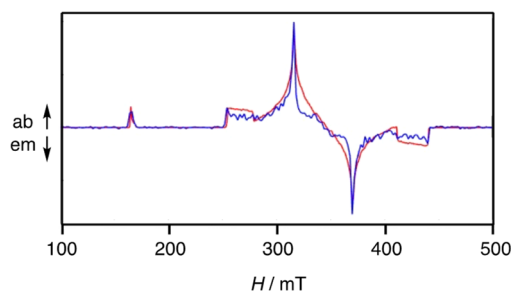

Figure 9. Time-resolved EPR spectra of PD-H crystals observed at 0.3 μs after 355 nm laser irradiation at 80 K. Microwave frequency was 9.740 GHz. Blue and red curves are observed and simulated spectra, respectively. The details of fitting parameters are given in the Supporting Information (Figures S9 and S10).

-0.087 cm^{-1} < 0, different from PP derivative (0.052 cm^{-1}),[73] is reasonable owing to the existence of quaternary carbon in the PD core. However, the preliminary results also suggested that ^{3}PD-H* is formed not via SF of ^{1}PD-H* but via ISC even though the energy requirement for SF, $E_S > 2E_T$, is satisfied (see Table 1). The lack of SF process is probably related to the rapid conformational change that leads to the ISC to T$_{n \geq 2}$. To ascertain whether these PDs undergo SF, more detailed ultrafast time-resolved absorption, luminescence, and EPR studies of films, crystals, and/or aggregates are needed.

CONCLUSIONS

In the investigation described above, we prepared and characterized the diphenyldihydropentalenediones PD-H, PD-OCH$_3$, and PD-CF$_3$ as a new class of large ΔE_{ST} compounds. The results of spectroscopic measurements suggest that PD-H has E_S and E_T values of 2.88 and 1.43 eV, respectively. Therefore, as anticipated, this substance has ΔE_{ST} and E_T values that are large and that satisfy the energetic requirements ($E_S > 2E_T$) for SF. The large ΔE_{ST} value is likely a consequence of (1) the presence of increased molecular planarity of the ring fused-diene subunit and (2) the avoidance of the resonance by the lack of amide groups in the dihydropentalenedione core. The low Φ_{FL} and the short τ_{FL}

of PD-H and PD-CF$_3$ crystals suggest the existence of rapid S$_1$ quenching processes by not only involving ISC but also including SF. Moreover, we demonstrated that substitution of electron-donating and -withdrawing groups on benzene rings of PD-H can be used to modulate E_S and E_T. Additionally, analysis of transient absorption data show that ^{3}PD-H*, ^{3}PD-OCH$_3$*, and ^{3}PD-CF$_3$* have excited triplet state lifetimes up to 118 μs. A combination of the observation made in this effort suggest that the strategy involving incorporation of a fused-diene subunit and removal of the possibility of the resonance observed for PP-Th is effective in designing substance that have large ΔE_{ST} and E_T values. It is significant that substances with high triplet energies have the potential of being utilized not only in optoelectronic applications but also in organic electronics. We are now conducting a careful investigation to determine if PD-H and its derivatives undergo SF.

■ ASSOCIATED CONTENT

Ⓢ Supporting Information

The Supporting Information is available free of charge at https://pubs.acs.org/doi/10.1021/acsomega.2c05341.

General; preparation of substances; X-ray crystallographic analysis; deconvolution of UV−vis absorption and FL spectra; supplementary photophysical properties; time-resolved electron paramagnetic resonance analysis; cyclic voltammetry; differential scanning calorimetry; theoretical calculations; ^{1}H, ^{13}C, and ^{19}F NMR spectra; and references (PDF)

Crystallographic data of PD-H (CIF)

Crystallographic data of PD-OCH$_3$ (CIF)

Crystallographic data of PD-CF$_3$ (CIF)

Cartesian coordinates of optimized geometry of PD-H (XYZ)

Cartesian coordinates of optimized geometry of PD-OCH$_3$ (XYZ)

Cartesian coordinates of optimized geometry of PD-CF$_3$ (XYZ)

(PDF)

■ AUTHOR INFORMATION

Corresponding Authors

Yasunori Matsui − *Department of Applied Chemistry, Graduate School of Engineering and The Research Institute for Molecular Electronic Devices (RIMED), Osaka Metropolitan University, Sakai, Osaka 599-8531, Japan;* ⓘ orcid.org/0000-0002-7719-0071; Email: matsui_yasunori@omu.ac.jp

Hiroshi Ikeda − *Department of Applied Chemistry, Graduate School of Engineering and The Research Institute for Molecular Electronic Devices (RIMED), Osaka Metropolitan University, Sakai, Osaka 599-8531, Japan;* ⓘ orcid.org/0000-0002-8161-2177; Email: hiroshi_ikeda@omu.ac.jp

Authors

Tomoki Nagaoka − *Department of Applied Chemistry, Graduate School of Engineering, Osaka Prefecture University, Sakai, Osaka 599-8531, Japan*

Masaaki Fuki − *Molecular Photoscience Research Center, Kobe University, Kobe, Hyogo 657-8501, Japan*

Takuya Ogaki − *Department of Applied Chemistry, Graduate School of Engineering and The Research Institute for Molecular Electronic Devices (RIMED), Osaka Metropolitan*

University, Sakai, Osaka 599-8531, Japan; ● orcid.org/0000-0003-2639-141X

Eisuke Ohta − *Department of Applied Chemistry, Graduate School of Engineering, Osaka Prefecture University, Sakai, Osaka 599-8531, Japan*

Yasuhiro Kobori − *Molecular Photoscience Research Center and Graduate School of Science, Kobe University, Kobe, Hyogo 657-8501, Japan;* ● orcid.org/0000-0001-8370-9362

Complete contact information is available at:
https://pubs.acs.org/10.1021/acsomega.2c05341

Notes
The authors declare no competing financial interest.

■ ACKNOWLEDGMENTS

■ REFERENCES

(1) Uoyama, H.; Goushi, K.; Shizu, K.; Nomura, H.; Adachi, C. Highly Efficient Organic Light-emitting Diodes from Delayed Fluorescence. *Nature* **2012**, *492*, 234−238.

(2) Yang, Z.; Mao, Z.; Xie, Z.; Zhang, Y.; Liu, S.; Zhao, J.; Xu, J.; Chi, Z.; Aldred, M. P. Recent Advances in Organic Thermally Activated Delayed Fluorescence Materials. *Chem. Soc. Rev.* **2017**, *46*, 915−1016.

(3) Monguzzi, A.; Mezyk, J.; Scotognella, F.; Tubino, R.; Meinardi, F. Upconversion-induced Fluorescence in Multicomponent Systems: Steady-State Excitation Power Threshold. *Phys. Rev. B: Condens. Matter Mater. Phys.* **2008**, *78*, 195112.

(4) Zhou, J.; Liu, Q.; Feng, W.; Sun, Y.; Li, F. Upconversion Luminescent Materials: Advances and Applications. *Chem. Rev.* **2015**, *115*, 395−465.

(5) Singh-Rachford, T. N.; Castellano, F. N. Photon Upconversion Based on Sensitized Triplet−Triplet Annihilation. *Coord. Chem. Rev.* **2010**, *254*, 2560−2573.

(6) Pun, A. B.; Campos, L. M.; Congreve, D. N. Tunable Emission from Triplet Fusion Upconversion in Diketopyrrolopyrroles. *J. Am. Chem. Soc.* **2019**, *141*, 3777−3781.

(7) Smith, M. B.; Michl, J. Singlet Fission. *Chem. Rev.* **2010**, *110*, 6891−6936.

(8) Wang, L.; Bai, S.; Wu, Y.; Liu, Y.; Yao, J.; Fu, H. Revealing the Nature of Singlet Fission under the Veil of Internal Conversion. *Angew. Chem., Int. Ed.* **2020**, *59*, 2003−2007.

(9) Miyata, K.; Conrad-Burton, F. S.; Geyer, F. L.; Zhu, X.-Y. Triplet Pair States in Singlet Fission. *Chem. Rev.* **2019**, *119*, 4261−4292.

(10) Weiss, L. R.; Bayliss, S. L.; Kraffert, F.; Thorley, K. J.; Anthony, J. E.; Bittl, R.; Friend, R. H.; Rao, A.; Greenham, N. C.; Behrends, J. Strongly Exchange-coupled Triplet Pairs in an Organic Semiconductor. *Nat. Phys.* **2017**, *13*, 176−181.

(11) Tayebjee, M. J. Y.; Sanders, S. N.; Kumarasamy, E.; Campos, L. M.; Sfeir, M. Y.; McCamey, D. R. Quintet Multiexciton Dynamics in Singlet Fission. *Nat. Phys.* **2017**, *13*, 182−188.

(12) Einzinger, M.; Wu, T.; Kompalla, J. F.; Smith, H. L.; Perkinson, C. F.; Nienhaus, L.; Wieghold, S.; Congreve, D. N.; Kahn, A.; Bawendi, M. G.; Baldo, M. A. Sensitization of Silicon by Singlet Exciton Fission in Tetracene. *Nature* **2019**, *571*, 90−94.

(13) MacQueen, R. W.; Liebhaber, M.; Niederhausen, J.; Mews, M.; Gersmann, C.; Jäckle, S.; Jäger, K.; Tayebjee, M. J. Y.; Schmidt, T. W.;

(14) Rech, B.; Lips, K. Crystalline Silicon Solar Cells with Tetracene Interlayers: The Path to Silicon-Singlet Fission Heterojunction Devices. *Mater. Horiz.* **2018**, *5*, 1065−1075.

(14) Ullrich, T.; Munz, D.; Guldi, D. M. Unconventional Singlet Fission Materials. *Chem. Soc. Rev.* **2021**, *50*, 3485−3518.

(15) Japahuge, A.; Zeng, T. Theoretical Studies of Singlet Fission: Searching for Materials and Exploring Mechanisms. *ChemPlusChem* **2018**, *83*, 146−182.

(16) Minami, T.; Ito, S.; Nakano, M. Theoretical Study of Singlet Fission in Oligorylenes. *J. Phys. Chem. Lett.* **2012**, *3*, 2719−2723.

(17) Blaskovits, J. T.; Fumanal, M.; Vela, S.; Cho, Y.; Corminboeuf, C. Heteroatom Oxidation Controls Singlet−Triplet Energy Splitting in Singlet Fission Building Blocks. *Chem. Commun.* **2022**, *58*, 1338−1341.

(18) Nakamura, S.; Sakai, H.; Nagashima, H.; Kobori, Y.; Tkachenko, N. V.; Hasobe, T. Quantitative Sequential Photoenergy Conversion Process from Singlet Fission to Intermolecular Two-electron Transfers Utilizing Tetracene Dimer. *ACS Energy Lett.* **2019**, *4*, 26−31.

(19) Jacobberger, R. M.; Qiu, Y.; Williams, M. L.; Krzyaniak, M. D.; Wasielewski, M. R. Using Molecular Design to Enhance the Coherence Time of Quintet Multiexcitons Generated by Singlet Fission in Single Crystals. *J. Am. Chem. Soc.* **2022**, *144*, 2276−2283.

(20) Wang, L.; Cai, W.; Sun, J.; Wu, Y.; Zhang, B.; Tian, X.; Guo, S.; Liang, W.; Fu, H.; Yao, J. H-Type-like Aggregation-accelerated Singlet Fission Process in Dipyrrolonaphthyridinedione Thin Film: The Role of Charge Transfer/Excimer Mixed Intermediate State. *J. Phys. Chem. Lett.* **2021**, *12*, 12276−12282.

(21) Bae, Y. J.; Zhao, X.; Kryzaniak, M. D.; Nagashima, H.; Strzalka, J.; Zhang, Q.; Wasielewski, M. R. Spin Dynamics of Quintet and Triplet States Resulting from Singlet Fission in Oriented Terrylene-diimide and Quaterrylenediimide Films. *J. Phys. Chem. C* **2020**, *124*, 9822−9833.

(22) Wang, L.; Zhang, T.-S.; Fu, L.; Xie, S.; Wu, Y.; Cui, G.; Fang, W.-H.; Yao, J.; Fu, H. High-Lying 3^1A_g Dark-State-Mediated Singlet Fission. *J. Am. Chem. Soc.* **2021**, *143*, 5691−5697.

(23) Wang, L.; Lin, L.; Yang, J.; Wu, Y.; Wang, H.; Zhu, J.; Yao, J.; Fu, H. Singlet Fission in a Pyrrole-fused Cross-conjugated Skeleton with Adaptive Aromaticity. *J. Am. Chem. Soc.* **2020**, *142*, 10235−10239.

(24) Imahori, H.; Kobori, Y.; Kaji, H. Manipulation of Charge-Transfer States by Molecular Design: Perspective from "Dynamic Exciton". *Acc. Mater. Res.* **2021**, *2*, 501−514.

(25) Fallon, K. J.; Budden, P.; Salvadori, E.; Ganose, A. M.; Savory, C. N.; Eyre, L.; Dowland, S.; Ai, Q.; Goodlett, S.; Risko, C.; Scanlon, D. O.; Kay, C. W. M.; Rao, A.; Friend, R. H.; Musser, A. J.; Bronstein, H. Exploiting Excited-State Aromaticity To Design Highly Stable Singlet Fission Materials. *J. Am. Chem. Soc.* **2019**, *141*, 13867−13876.

(26) Mukhopadhyay, T.; Musser, A. J.; Puttaraju, B.; Dhar, J.; Friend, R. H.; Patil, S. Is the Chemical Strategy for Imbuing "Polyene" Character in Diketopyrrolopyrrole-based Chromophores Sufficient for Singlet Fission? *J. Phys. Chem. Lett.* **2017**, *8*, 984−991.

(27) Matsui, Y.; Kawaoka, S.; Nagashima, H.; Nakagawa, T.; Okamura, N.; Ogaki, T.; Ohta, E.; Akimoto, S.; Sato-Tomita, A.; Yagi, S.; Kobori, Y.; Ikeda, H. Exergonic Intramolecular Singlet Fission of an Adamantane-linked Tetracene Dyad via Twin Quintet Multi-excitons. *J. Phys. Chem. C* **2019**, *123*, 18813−18823.

(28) Okil, M.; Salem, M. S.; Abdolkader, T. M.; Shaker, A. From Crystalline to Low-Cost Silicon-based Solar Cells: A Review. *Silicon* **2021**, *14*, 1895−1911.

(29) Liu, A. Y.; Phang, S. P.; Macdonald, D. Gettering in Silicon Photovoltaics: A Review. *Sol. Energy Mater. Sol. Cells* **2022**, *234*, 111447.

(30) Kojima, A.; Teshima, K.; Shirai, Y.; Miyasaka, T. Organometal Halide Perovskites as Visible-Light Sensitizers for Photovoltaic Cells. *J. Am. Chem. Soc.* **2009**, *131*, 6050−6051.

(31) Numata, Y.; Shibayama, N.; Miyasaka, T. FAPbBr₃ Perovskite Solar Cells with: V_{OC} Values over 1.5 V by Controlled Crystal Growth Using Tetramethylenesulfoxide. *J. Mater. Chem. A* **2022**, *10*, 672−681.

(32) Turro, N. J.; Ramamurthy, V.; Scaiano, J. C. Principles of Molecular Photochemistry: An Introduction; University Science Books, 2009.

(33) Matsuda, S.; Oyama, S.; Kobori, Y. Electron Spin Polarization Generated by Transport of Singlet and Quintet Multiexcitons to Spin-Correlated Triplet Pairs during Singlet Fissions. *Chem. Sci.* **2020**, *11*, 2934−2942.

(34) Nagashima, H.; Kawaoka, S.; Akimoto, S.; Tachikawa, T.; Matsui, Y.; Ikeda, H.; Kobori, Y. Singlet-Fission-Born Quintet State: Sublevel Selections and Trapping by Multiexciton Thermodynamics. *J. Phys. Chem. Lett.* **2018**, *9*, 5855−5861.

(35) Hudson, R. J.; Huang, D. M.; Kee, T. W. Anisotropic Triplet Exciton Diffusion in Crystalline Functionalized Pentacene. *J. Phys. Chem. C* **2020**, *124*, 23541−23550.

(36) Musser, A. J.; Maiuri, M.; Brida, D.; Cerullo, G.; Friend, R. H.; Clark, J. The Nature of Singlet Exciton Fission in Carotenoid Aggregates. *J. Am. Chem. Soc.* **2015**, *137*, 5130−5139.

(37) Quaranta, A.; Krieger-Liszkay, A.; Pascal, A. A.; Perreau, F.; Robert, B.; Vengris, M.; Llansola-Portoles, M. J. Singlet Fission in Naturally-organized Carotenoid Molecules. *Phys. Chem. Chem. Phys.* **2021**, *23*, 4768−4776.

(38) Chang, H.-T.; Chang, Y.-Q.; Han, R.-M.; Wang, P.; Zhang, J.-P.; Skibsted, L. H. Singlet Fission Reaction of Light-exposed β-Carotene Bound to Bovine Serum Albumin. A Novel Mechanism in Protection of Light-exposed Tissue by Dietary Carotenoids. *J. Agric. Food Chem.* **2017**, *65*, 6058−6062.

(39) Dillon, R. J.; Piland, G. B.; Bardeen, C. J. Different Rates of Singlet Fission in Monoclinic versus Orthorhombic Crystal Forms of Diphenylhexatriene. *J. Am. Chem. Soc.* **2013**, *135*, 17278−17281.

(40) Ishikawa, K.; Yago, T.; Wakasa, M. Exploring the Structure of an Exchange-Coupled Triplet Pair Generated by Singlet Fission in Crystalline Diphenylhexatriene: Anisotropic Magnetic Field Effects on Fluorescence in High Fields. *J. Phys. Chem. C* **2018**, *122*, 22264−22272.

(41) Vogeler, F.; Siegert, S.; Marian, C. M.; Weinkauf, R. T_1, T_2 State Energies and Electron Affinities of Small α,ω-Diphenylpolyenes Investigated by Anion Photodetachment Photoelectron Spectroscopy and Excited-State Theory. *ChemPhysChem* **2011**, *12*, 1948−1956.

(42) Sonoda, Y.; Morii, H.; Sakuragi, M.; Suzuki, Y. Substituent Effect on the *cis-trans* Photoisomerization of *trans,trans,trans*-1,6-Diphenyl-1,3,5-hexatrienes. *Chem. Lett.* **1998**, *27*, 349−350.

(43) Sonoda, Y. Solid-State [2+2] Photodimerization and Photo-polymerization of α,ω-Diarylpolyene Monomers: Effective Utilization of Noncovalent Intermolecular Interactions in Crystals. *Molecules* **2010**, *16*, 119−148.

(44) Hartnett, P. E.; Margulies, E. A.; Mauck, C. M.; Miller, S. A.; Wu, Y.; Wu, Y. L.; Marks, T. J.; Wasielewski, M. R. Effects of Crystal Morphology on Singlet Exciton Fission in Diketopyrrolopyrrole Thin Films. *J. Phys. Chem. B* **2016**, *120*, 1357−1366.

(45) Shi, H.; Sun, W.; Wang, Q.; Gu, G.; Si, W.; Huang, W.; Zhang, Q.; Dong, X. A Thienyl-substituted Diketopyrrolopyrrole Derivative with Efficient Reactive Oxygen Species Generation for Photodynamic Therapy. *ChemPlusChem* **2016**, *81*, 515−520.

(46) Frisch, M. J.; Trucks, G. W.; Schlegel, H. B.; Scuseria, G. E.; Robb, M. A.; Cheeseman, J. R.; Scalmani, G.; Barone, V.; Mennucci, B.; Petersson, G. A.; Nakatsuji, H.; Caricato, M.; Li, X.; Hratchian, H. P.; Izmaylov, A. F.; Bloino, J.; Zheng, G.; Sonnenberg, J. L.; Hada, M.; Ehara, M.; Toyota, K.; Fukuda, R.; Hasegawa, J.; Ishida, M.; Nakajima, T.; Honda, Y.; Kitao, O.; Nakai, H.; Vreven, T.; Montgomery, J. A.; Peralta, J. E.; Ogliaro, F.; Bearpark, M.; Heyd, J. J.; Brothers, E.; Kudin, K. N.; Staroverov, V. N.; Kobayashi, R.; Normand, J.; Raghavachari, K.; Rendell, A.; Burant, J. C.; Iyengar, S. S.; Tomasi, J.; Cossi, M.; Rega, N.; Millam, J. M.; Klene, M.; Knox, J. E.; Cross, J. B.; Bakken, V.; Adamo, C.; Jaramillo, J.; Gomperts, R.; Stratmann, R. E.; Yazyev, O.; Austin, A. J.; Cammi, R.; Pomelli, C.; Ochterski, J. W.; Martin, R. L.; Morokuma, K.; Zakrzewski, V. G.; Voth, G. A.; Salvador, P.; Dannenberg, J. J.; Dapprich, S.; Daniels, A. D.; Farkas, Ö.; Foresman, J. B.; Ortiz, J. V.; Cioslowski, J.; Fox, D. J. *Gaussian 09*; Gaussian, Inc., 2009.

(47) Sheldrick, G. M. SHELXT- Integrated Space-group and Crystal-structure Determination. *Acta Crystallogr., Sect. A: Found. Adv.* **2015**, *71*, 3−8.

(48) Sheldrick, G. M. Crystal Structure Refinement with SHELXL. *Acta Crystallogr., Sect. C: Struct. Chem.* **2015**, *71*, 3−8.

(49) Dolomanov, O. V.; Bourhis, L. J.; Gildea, R. J.; Howard, J. A. K.; Puschmann, H. OLEX2 : A Complete Structure Solution, Refinement and Analysis Program. *J. Appl. Crystallogr.* **2009**, *42*, 339−341.

(50) McGlynn, S. P.; Azumi, T.; Kasha, M. External Heavy-Atom Spin—Orbital Coupling Effect. V. Absorption Studies of Triplet States. *J. Chem. Phys.* **1964**, *40*, 507−515.

(51) Saito, Y.; Higuchi, M.; Yoshioka, S.; Senboku, H.; Inokuma, Y. Bioinspired Synthesis of Pentalene-based Chromophores from an Oligoketone Chain. *Chem. Commun.* **2018**, *54*, 6788−6791.

(52) Inagaki, S.; Saito, K.; Suto, S.; Aihara, H.; Sugawara, A.; Tamura, S.; Kawano, T. Synthesis of 5-Aryl-3(2*H*)-furanones Using Intramolecular Cyclization of Sulfonium Salts. *J. Org. Chem.* **2018**, *83*, 13834−13846.

(53) Xu, Q.; Qi, H.; Sun, M.; Zuo, D.; Jiang, X.; Wen, Z. Synthesis and Biological Evaluation of 3-Alkyl-1,5-diaryl-1*H*-pyrazoles as Rigid Analogues of Combretastatin A-4 with Potent Antiproliferative Activity. *PLoS One* **2015**, *10*, No. e0128710.

(54) Davis, B. R.; Hinds, M. G.; Ting, P. P. C. Clemmensen Reduvtion. X The Synthesis and Acidolysis of Some Aryl Alkyl Substituted Cyclopropane-1,2-diols. *Aust. J. Chem.* **1992**, *45*, 856−875.

(55) Tirpak, R. E.; Rathke, M. W. Acylation of Ketone Silyl Enol Ethers with Acid Chlorides. Synthesis of 1,3-Diketones. *J. Org. Chem.* **1982**, *47*, 5099−5102.

(56) Adam, W.; Heidenfelder, T.; Sahin, C. Diastereo- and Regioselective Synthesis of Diquinanes and Related Systems from Tricyclo[3.3.0.0^{2,4}]octanes by Chemical Electron Transfer (CET). *Synthesis* **1995**, *1995*, 1163−1170.

(57) Uesaka, M.; Saito, Y.; Yoshioka, S.; Domoto, Y.; Fujita, M.; Inokuma, Y. Oligoacetylacetones as Shapable Carbon Chains and Their Transformation to Oligoimines for Construction of Metal-Organic Architectures. *Commun. Chem.* **2018**, *1*, 23.

(58) Amarnath, V.; Amarnath, K. Intermediates in the Paal−Knorr Synthesis of Furans. *J. Org. Chem.* **1995**, *60*, 301−307.

(59) Karsten, B. P.; Bouwer, R. K. M.; Hummelen, J. C.; Williams, R. M.; Janssen, R. A. J. Charge Separation and (Triplet) Recombination in Diketopyrrolopyrrole−Fullerene Triads. *Photochem. Photobiol. Sci.* **2010**, *9*, 1055−1065.

(60) Bhattacharyya, K.; Datta, A. Polymorphism Controlled Singlet Fission in TIPS-Anthracene: Role of Stacking Orientation. *J. Phys. Chem. C* **2017**, *121*, 1412−1420.

(61) Buchanan, E. A.; Kaleta, J.; Wen, J.; Lapidus, S. H.; Císařová, I.; Havlas, Z.; Johnson, J. C.; Michl, J. Molecular Packing and Singlet Fission: The Parent and Three Fluorinated 1,3-Diphenylisobenzofurans. *J. Phys. Chem. Lett.* **2019**, *10*, 1947−1953.

(62) Wang, X.; Garcia, T.; Monaco, S.; Schatschneider, B.; Marom, N. Effect of Crystal Packing on the Excitonic Properties of Rubrene Polymorphs. *CrystEngComm* **2016**, *18*, 7353−7362.

(63) Rais, D.; Toman, P.; Pfleger, J.; Acharya, U.; Panthi, Y. R.; Menšík, M.; Zhigunov, A.; Thottappali, M. A.; Vala, M.; Marková, A.; Stříteský, S.; Weiter, M.; Cigánek, M.; Krajčovič, J.; Pauk, K.; Imramovský, A.; Zaykov, A.; Michl, J. Singlet Fission in Thin Solid Films of Bis(thienyl)diketopyrrolopyrroles. *ChemPlusChem* **2020**, *85*, 2689−2703.

(64) Kato, M.; Ito, H.; Hasegawa, M.; Ishii, K. Soft Crystals: Flexible Response Systems with High Structural Order. *Chem.—Eur. J.* **2019**, *25*, 5105−5112.

(65) Murov, S. L.; Carmichael, I.; Hug, G. L. *Handbook of Photochemistry*, 2nd ed.; Marcel Dekker: New York, 2002; Vol. 78.

(66) Eguchi, M.; Shimada, T.; Inoue, H.; Takagi, S. Kinetic Analysis by Laser Flash Photolysis of Porphyrin Molecules' Orientation Change at the Surface of Silicate Nanosheet. *J. Phys. Chem. C* **2016**, *120*, 7428−7434.

(67) Marets, N.; Kanno, S.; Ogata, S.; Ishii, A.; Kawaguchi, S.; Hasegawa, M. Lanthanide-Oligomeric Brush Films: From Luminescence Properties to Structure Resolution. *ACS Omega* **2019**, *4*, 15512−15520.

(68) Akune, Y.; Hirosawa, R.; Endo, N.; Hatano, S.; Hosokai, T.; Sato, H.; Matsumoto, S. Tuning of Fluorescence Efficiency via Local Modification of the Crystal Structure by Benzyl Groups in Polymorphs of a Pyrazine Dye. *CrystEngComm* **2017**, *19*, 1947−1952.

(69) Luo, J.; Xie, Z.; Lam, J. W. Y.; Cheng, L.; Tang, H.; Chen, C.; Qiu, H. S.; Kwok, X.; Zhan, Y.; Liu, D.; Zhu, B. Z. Aggregation-induced Emission of 1-Methyl-1,2,3,4,5-pentaphenylsilole. *Chem. Commun.* **2001**, 1740−1741.

(70) Tong, H.; Hong, Y.; Dong, Y.; Häußler, M.; Lam, J. W. Y.; Li, Z.; Guo, Z.; Guo, Z.; Tang, B. Z. Fluorescent "Light-up" Bioprobes Based on Tetraphenylethylene Derivatives with Aggregation-induced Emission Characteristics. *Chem. Commun.* **2006**, 3705−3707.

(71) Burdett, J. J.; Bardeen, C. J. Quantum Beats in Crystalline Tetracene Delayed Fluorescence Due to Triplet Pair Coherences Produced by Direct Singlet Fission. *J. Am. Chem. Soc.* **2012**, *134*, 8597−8607.

(72) Dover, C. B.; Gallaher, J. K.; Frazer, L.; Tapping, P. C.; Petty, A. J.; Crossley, M. J.; Anthony, J. E.; Kee, T. W.; Schmidt, T. W. Endothermic Singlet Fission Is Hindered by Excimer Formation. *Nat. Chem.* **2018**, *10*, 305−310.

(73) Salvadori, E.; Luke, N.; Shaikh, J.; Leventis, A.; Bronstein, H.; Kay, C. W. M.; Clarke, T. M. Ultra-fast Spin-mixing in a Diketopyrrolopyrrole Monomer/Fullerene Blend Charge Transfer State. *J. Mater. Chem. A* **2017**, *5*, 24335−24343.